Journal of Metals, Materials and Minerals, 35(3), e2318, 2025

Synthesis temperature-driven enhancements in BiOI photocatalysis: A hydrothermal approach

Sorawit THUEANBANGYANG[1], Kittiyaporn SINGSUMPHAN[1], Varunya ATIMAYULERD[1], Chutima NAKMUK[1], Cheewita SUWANCHAWALIT[2], and Montri AIEMPANAKIT[1,*]

[1] *Department of Physics, Faculty of Science, Silpakorn University, Thailand*
[2] *Department of Chemistry, Faculty of Science, Silpakorn University, Thailand*

***Corresponding author e-mail**: aiempanakit_m@su.ac.th

Received date:
18 February 2025
Revised date:
26 March 2025
Accepted date:
1 May 2025

Keywords:
Bismuth oxoiodide (BiOI);
Hydrothermal synthesis;
Photocatalysis;
Visible light;
Indigo carmine degradation

Abstract

Bismuth oxyiodide (BiOI) is a promising photocatalyst for visible-light-driven environmental remediation. However, its photocatalytic efficiency is highly dependent on synthesis conditions, particularly hydrothermal temperature, which governs its structural, optical, and electronic properties. In this study, BiOI was synthesized via a hydrothermal method at temperatures of 120°C, 150°C, 180°C, and 210°C to investigate the effect of temperature on its photocatalytic performance systematically. Comprehensive characterizations, including X-ray diffraction, field emission scanning electron microscopy, energy-dispersive X-ray spectroscopy, Fourier-transform infrared spectroscopy, UV-vis diffuse reflectance spectroscopy, photoluminescence and photocatalytic degradation studies, were conducted to analyze crystallinity, morphology, band structure and charge transfer properties. The results demonstrated that BiOI synthesized at 180°C exhibited an optimal combination of crystallinity and particle dispersion, which enhanced charge separation and photocatalytic activity. It achieved a degradation efficiency of 94% for indigo carmine within 60 min under visible light irradiation. The bandgap energy and electronic structure of BiOI played a critical role in determining the dominant reactive species, with superoxide radicals ($^{\bullet}O_2^-$) being the primary contributors to indigo carmine degradation. The study provides new insights into the relationship between synthesis temperature, structural evolution, and photocatalytic efficiency, offering a scalable and effective approach for optimizing BiOI-based photocatalysts for environmental applications.

1. Introduction

Water pollution is one of the most pressing global challenges, with industrial effluents, pharmaceuticals, and synthetic dyes contributing to severe environmental contamination [1-6]. Conventional wastewater treatment methods often fall short of completely degrading persistent organic pollutants [7], necessitating the development of more effective and sustainable alternatives. Semiconductor-based photocatalysis has emerged as a promising approach, offering the ability to harness solar energy for pollutant degradation without generating secondary waste [8].

Bismuth oxyiodide (BiOI) has attracted attention as a visible-light-active photocatalyst due to its narrow bandgap energy (1.72 eV to 2.0 eV), enabling strong light absorption and efficient charge carrier generation [9-11], making it suitable for environmental remediation applications [12-14]. Various strategies have been explored to enhance its photocatalytic efficiency, including heterojunction formation, elemental doping, and nanostructure engineering [15-17]. Heterojunction-based approaches, such as coupling BiOI with BiOCl [18], $BiVO_4$ [19], or Ag-based materials [20], have enhanced charge separation and extended carrier lifetimes [21]. While these approaches have led to significant efficiency improvements, they often involve complex synthesis processes, increased costs, and potential stability issues over time [22]. An alternative, more practical approach involves optimizing synthesis parameters rather than introducing chemical modifications. Recent trends in materials science emphasize the need for scalable, cost-effective, and stable photocatalysts [23-25]. Hydrothermal synthesis allows controlled crystallinity and morphology, directly influencing photocatalytic efficiency [26,27]. Despite its advantages, the effect of hydrothermal temperature on BiOI's structural and optical properties remains inadequate [28]. Moreover, its recyclability, crucial for real-world applications, has not been widely explored, as most studies have only examined its initial photocatalytic performance [29].

This study systematically investigates the impact of hydrothermal synthesis temperature (120°C, 150°C, 180°C, and 210°C) on the structural, optical, and photocatalytic properties of BiOI. Unlike previous studies that relied on heterojunctions or elemental doping, this work focuses solely on synthesis optimization to improve performance. By avoiding chemical modifications, this approach preserves BiOI's intrinsic stability and simplifies large-scale production. Moreover, optimizing synthesis temperature aligns with the principles of green chemistry, reducing the need for additional reagents while maintaining strong photocatalytic activity. Beyond improving initial photocatalytic performance, this study also assesses the recyclability of BiOI synthesized under optimal conditions to evaluate its long-term applicability for wastewater treatment. While prior research has emphasized BiOI's efficiency in single-use applications, few studies have examined its durability over multiple cycles. By addressing this gap, this work

provides valuable insights into the role of hydrothermal temperature in tuning BiOI's properties. It offers a cost-effective, scalable strategy for developing high-performance photocatalysts for environmental remediation.

2. Experimental

2.1 Preparation of BiOI

All chemicals used in this study were of analytical grade. BiOI was synthesized via the hydrothermal method using bismuth (III) nitrate pentahydrate ($Bi(NO_3)_3 \cdot 5H_2O$) and potassium iodide (KI) as precursors. Initially, 1 mmol (2.4253 g) of $Bi(NO_3)_3 \cdot 5H_2O$ was dissolved in 100 mL of 2 M nitric acid (HNO_3), and 2 mmol (1.61 g) of KI was dissolved in 100 mL of deionized water separately. The $Bi(NO_3)_3$ and KI solutions were mixed, and the pH of the resulting solution was adjusted to 10 by adding 2 M sodium hydroxide (NaOH) solution, followed by continuous stirring for 1 h to ensure homogeneous mixing.

The prepared solution was then transferred to a Teflon-lined stainless-steel autoclave and subjected to hydrothermal treatment at four different temperatures (120°C, 150°C, 180°C, and 210°C) for 5 h. After completion, the autoclave was allowed to cool naturally to room temperature. The orange-colored BiOI precipitate was filtered (0.1 µm filter), washed twice with deionized water, and dried at 80°C overnight. The synthesis process is summarized in Figure 1.

2.2 Characterizations

The crystalline structure of the synthesized BiOI was analyzed using X-ray diffraction (XRD, Malvern Panalytical, Aeris) with a CuKα radiation source (40 kV, 8 mA), scanning in the 20° to 80° diffraction range to confirm phase purity and crystallinity. The surface morphology and particle size were examined using field emission scanning electron microscopy (FE-SEM, Tescan, Mira 3). At the same time, the elemental composition was determined via energy-dispersive X-ray spectroscopy (EDX) to verify bismuth (Bi), oxygen (O), and iodine (I) distribution. The functional groups in BiOI were identified through Fourier transform infrared spectroscopy (FT-IR) (PerkinElmer, Frontier) using the attenuated total reflectance (ATR) technique in the 4000 cm^{-1} to 400 cm^{-1} range, providing insights into surface chemical bonds. Finally, optical properties, including bandgap energy and visible light absorption, were assessed using UV-vis diffuse reflectance spectroscopy (DRS, Shimadzu, UV-2600i), employing Tauc's plot analysis to estimate the bandgap, which is critical for photocatalytic applications. Photo-luminescence (PL, PerkinElmer Precisely LS 55) spectra were measured at room temperature using a luminescence spectrophotometer by using an excitation wavelength of 400 nm.

2.3 Photocatalytic experiment

The photocatalytic activity of the synthesized BiOI samples was evaluated by measuring the degradation of indigo carmine under visible light irradiation. A 0.050 g of BiOI was dispersed in 50 mL of indigo carmine solution with an initial concentration of 5.0×10^{-5} M. The mixture was stirred in the dark for 30 min to achieve adsorption desorption equilibrium. The suspension was then exposed to visible light using two PHILIPS TLD 18W/865 fluorescent lamps, and aliquots of 3 mL to 5 mL were collected at 15 min intervals for a total reaction time of 60 min. The collected samples were centrifuged to remove any remaining BiOI particles, and the filtrate was analyzed using a UV-vis spectrophotometer (Thermo-Orion, AquaMate 8000) at the maximum absorption wavelength of 610 nm.

The photocatalytic degradation efficiency was calculated using the Equation (1) [30].

$$\text{Photocatalytic degradation efficiency (\%)} = \frac{C_0 - C}{C_0} \times 100\% \quad (1)$$

Where C_0 and C represent the initial and final concentrations of indigo carmine at different time intervals, respectively. The degradation kinetics were analyzed using the first-order reaction model [31].

$$ln\left(\frac{C}{C_0}\right) = -kt \quad (2)$$

where k is the reaction rate constant, and t is the reaction time.

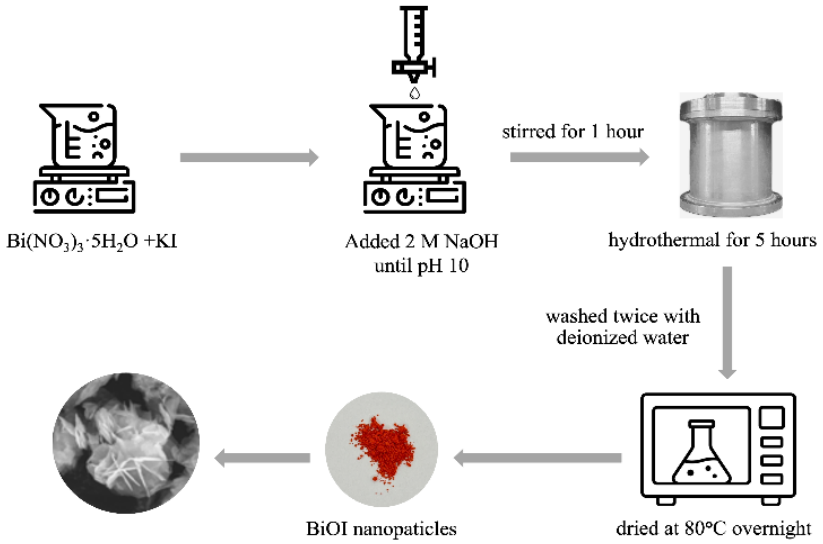

Figure 1. Schematic representation of BiOI synthesis via the hydrothermal method.

For active species trapping experiments, 0.1 M of ethylenediaminetetraacetic acid (EDTA), benzoquinone (BQ), and butanal were used as scavengers for holes (h^+), superoxide radicals ($^{\bullet}O_2^-$), and hydroxyl radicals ($^{\bullet}OH$), respectively. Each scavenger was added to the dye solution after stirring in the dark for 30 min to ensure saturation before light irradiation.

3. Results and discussion

3.1 X-ray diffraction and crystal size

The XRD analysis of BiOI synthesized via the hydrothermal process at temperatures of 120°C, 150°C, 180°C, and 210°C is presented in Figure 2. All diffraction peaks observed in the XRD patterns correspond well with the tetragonal BiOI (JCPDS card No. 10-0445 [27]), confirming the successful formation of the pure BiOI phase in all synthesized samples. Furthermore, the peak intensities increase as the hydrothermal temperature rises, indicating an improvement in crystallinity. Notably, the diffraction peaks become sharper and more intense at higher temperatures, especially at 210°C, suggesting better grain growth and reduced lattice defects. This trend indicates that higher synthesis temperatures enhance the degree of crystallization, leading to a more ordered atomic arrangement within the BiOI lattice. Despite the variations in peak intensity, all BiOI samples maintained a consistent phase composition without secondary phases or impurities, confirming the formation of pure BiOI.

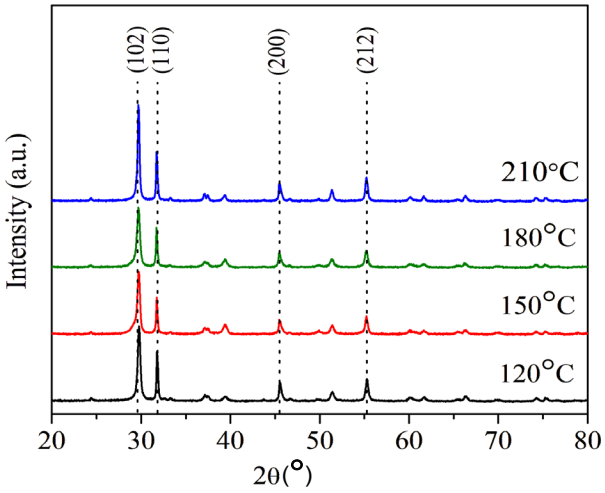

Figure 2. XRD patterns of BiOI synthesized at different hydrothermal temperatures. All observed peaks correspond to pure BiOI. Only representative peaks (102), (110), (200), and (212) are labeled to support a discussion of crystallite size and crystallinity.

To evaluate the impact of temperature on crystallite size (L), the Scherrer equation was applied.

$$L = \frac{K\lambda}{\beta \cos\theta} \tag{3}$$

where K is a constant dependent on crystal shape, normally used as 0.9, λ is the wavelength of X-ray (1.54060 Å), β is the width of the peak at half the maximum height in radians, and θ is the diffraction angle in degree. In this study, the crystallite size of BiOI was calculated using the Scherrer equation based on the diffraction peak at $2\theta = 29.6°$, corresponding to the (102) plane of tetragonal BiOI. the crystallite sizes of BiOI synthesized at different temperatures were calculated using this equation and are summarized in Table 1. The results show a clear trend of increasing crystallite size with rising hydrothermal temperature, where the crystallite size grows from 31.63 nm at 120°C to 47.44 nm at 210°C. Although not all diffraction peaks show a distinct trend, the (102) and (110) peaks exhibit increased intensity with rising synthesis temperature, suggesting improved crystallinity. These changes, along with the increase in calculated crystallite size, imply that higher temperatures promote better structural order in BiOI. This interpretation is consistent with previous studies [32], which report enhanced grain growth and atomic diffusion at elevated hydrothermal temperatures. These findings confirm that hydrothermal temperature significantly influences the crystallite size of BiOI, with higher temperatures leading to larger crystallites and improved structural order [26,28]. Notably, despite the increase in crystallite size, the XRD analysis alone does not provide information on the overall particle morphology or aggregation behavior. Therefore, further insights into the microstructural evolution of BiOI under different hydrothermal conditions are required, which will be analyzed using FE-SEM in the next section.

3.2 Surface morphology and EDX analysis

FE-SEM images (Figure 3) illustrate the morphological evolution of BiOI particles synthesized at different hydrothermal temperatures. At 120°C (Figure 3(a)), the BiOI particles exhibit a plate-like morphology with significant aggregation, forming large particle clusters. This aggregation is attributed to the limited atomic mobility at lower temperatures, which restricts grain growth and leads to particle agglomeration [28]. As the temperature increases to 150°C (Figure 3(b)), the particles become more dispersed, and individual plate-like structures are more visible, suggesting improved crystallization and reduced agglomeration. At 180°C (Figure 3(c)), the BiOI particles display a more distinct morphology with smaller and well-separated structures, indicating enhanced dissolution-recrystallization effects promoting

Table 1. Properties of BiOI synthesized at different hydrothermal temperatures.

BiOI sample	Crystal size [nm]	Bandgap energy [eV]	E_{VB} [eV]	E_{CB} [eV]
120°C	31.63	1.91	2.398	0.488
150°C	34.51	1.91	2.398	0.488
180°C	37.95	1.89	2.388	0.498
210°C	47.44	1.91	2.398	0.488

finer crystallite formation. Finally, at 210°C (Figure 3(d)), the particles exhibit the highest degree of dispersion with smaller, well-defined features. This result suggests that at higher temperatures, BiOI undergoes increased fragmentation of its plate-like structures, which enhances particle dispersion rather than forming larger aggregates. This trend aligns with the XRD results, which indicate a progressive increase in crystallite size with temperature. However, FE-SEM images reveal that while individual crystallites grow larger at higher temperatures, the particle clusters become smaller and more dispersed. This phenomenon can be attributed to enhanced thermal energy, which promotes grain growth while simultaneously reducing interparticle adhesion, leading to the fragmentation of larger clusters into finer structures. The increased atomic mobility at elevated temperatures facilitates crystallization but also contributes to breaking apart agglomerated BiOI particles, resulting in improved dispersion. This observation is consistent with previous studies, which have shown that increased synthesis temperatures enhance atomic diffusion, leading to reduced particle agglomeration and improved structural dispersion in BiOI materials [32]. Despite these morphological transformations, all BiOI samples retain their characteristic plate-like structure, confirming that hydrothermal temperature is crucial in modulating particle dispersion and growth without altering the fundamental BiOI crystal framework.

The elemental composition of the synthesized BiOI particles was further analyzed using EDX. The results, summarized in Table 2, confirm the presence of Bi, O, and I in all samples. Notably, the Bi/I atomic ratio of the sample synthesized at 180°C is close to the ideal 1:1 stoichiometry, while other samples show deviations of more than 10%. These variations may be attributed to surface inhomogeneity, incomplete precipitation, or limitations of the EDX technique, which provides semi-quantitative data based on localized surface analysis**.** Despite these differences, the elemental mapping confirmed uniform spatial distribution of the elements, suggesting overall successful synthesis, which aligns with previous studies on BiOI synthesized via hydrothermal methods [33].

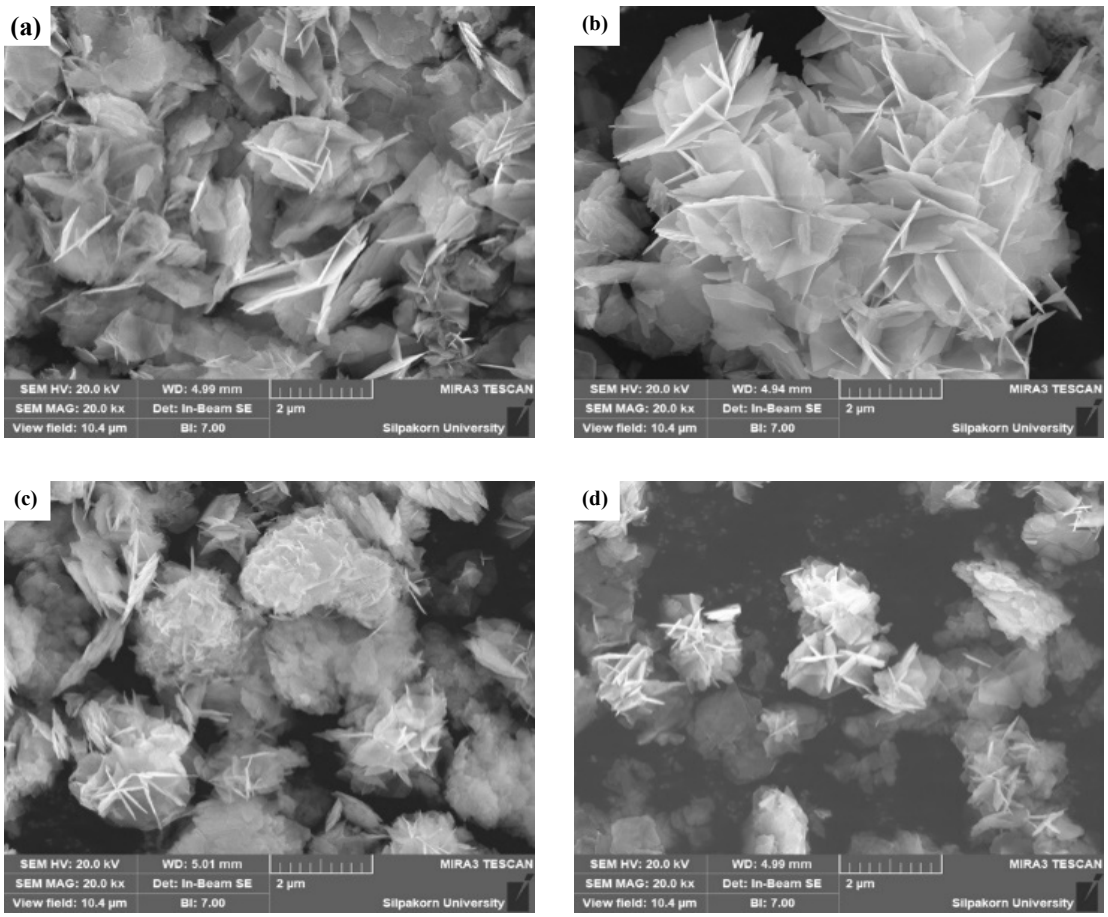

Figure 3. FE-SEM images of BiOI synthesized by hydrothermal process at (a) 120°C, (b) 150°C, (c) 180°C, and (d) 210°C.

Table 2. The EDX of BiOI synthesized by hydrothermal process at different temperatures.

BiOI sample	Bismuth atomic [%]	Oxygen atomic [%]	Iodine atomic [%]
120°C	30.23	45.08	24.69
150°C	28.23	36.32	35.45
180°C	35.73	29.91	34.36
210°C	33.27	40.41	26.31

3.3 FT-IR analysis

FT-IR spectroscopy was performed to analyze the structural and functional characteristics of BiOI synthesized at hydrothermal temperatures of 120°C, 150°C, 180°C, and 210°C, as shown in Figure 4. The FT-IR spectra exhibit characteristic absorption bands in the 400 cm^{-1} to 700 cm^{-1} region, corresponding to the stretching vibrations of Bi–O, Bi–O–I, and Bi–O–Bi bonds in the BiOI lattice [17]. These peaks confirm the formation of the BiOI phase and provide insight into the chemical bonding within the material. In addition, broad peaks observed in the range of 3500 cm^{-1} to 3000 cm^{-1} are attributed to O–H stretching vibrations, while the peak around 1600 cm^{-1} corresponds to the bending vibrations of the hydroxyl (–OH) groups [34,35]. These peaks indicate the presence of surface-adsorbed water molecules and hydroxyl groups, which can act as active sites for photocatalytic reactions. The bands observed between 1420 cm^{-1} belong to the stretching vibrations of the tetragonal crystal links of BiOI [36]. Additionally, weak absorption bands around 1720 cm^{-1} suggest the presence of carbonyl (C=O) [37], which may originate from atmospheric CO_2 adsorption or residual organic species from the synthesis process. Furthermore, characteristic C–H stretching vibrations in the aliphatic (2871 cm^{-1} to 2925 cm^{-1}) [38] regions could indicate surface contamination from environmental carbon sources or adsorbed organic species.

A notable trend observed in the FT-IR spectra is the gradual decrease in the intensity of the –OH-related peaks with increasing synthesis temperature. BiOI synthesized at lower temperatures, such as 120°C, exhibits broad and less defined peaks, which indicate higher impurity levels and incomplete crystallization, potentially hindering photocatalytic efficiency. In contrast, BiOI synthesized at 210°C shows sharp, well-defined peaks reflecting superior crystallinity and structural order. This trend is consistent with the XRD results, where higher synthesis temperatures promote improved crystallinity and structural order [19,27]. The reduction in surface hydroxyl (–OH) groups at elevated temperatures suggests decreased defect concentration, which may enhance charge separation. While surface hydroxyl groups can act as active sites in photocatalytic reactions, excessive hydroxylation may lead to charge recombination, reducing efficiency [35,39]. Therefore, optimizing the synthesis temperature is crucial for balancing crystallinity and surface chemistry to achieve maximum photocatalytic performance.

3.4 Optical properties

The optical properties of BiOI are crucial for its application in photocatalysis, as they determine the material's ability to absorb light and generate electron-hole pairs for catalytic reactions. The light absorption characteristics of BiOI synthesized via the hydrothermal process at temperatures of 120°C, 150°C, 180°C, and 210°C are presented in Figure 5(a). The absorption spectra indicate that all BiOI samples exhibit strong absorption within the visible light region, consistent with previous studies [19]. Among the synthesized samples, BiOI prepared at 150°C demonstrates the highest light absorption capacity, which may be attributed to the optimal balance between crystallinity and particle dispersion at this synthesis temperature. However, all samples retain the ability to absorb visible light efficiently, making them suitable for solar-driven photocatalytic applications. The bandgap energy of the BiOI samples was determined using Tauc's plot method, according to the equation.

$$(\alpha hv)^m = A(hv - E_g) \quad (4)$$

where α is the absorption coefficient, A is constant, hv is photon energy, E_g is the bandgap energy, and m depends on the type of transition (with $m = 2$ and 1/2 for direct and indirect allowed transitions, respectively). Since BiOI exhibits an indirect bandgap transition [36,40], the value of m was set to 1/2, and the bandgap energy was obtained by extrapolating the linear portion of the graph to the x-axis. The absorption coefficient (α) was estimated from UV-Vis absorbance data. The constant A in Equation (4) is a proportionality factor and was not explicitly calculated. Instead, E_g was determined using the standard method of extrapolating the linear portion of the $(\alpha hv)^{1/2}$ versus hv plot. Figure 5(b) presents the Tauc's plots for BiOI synthesized at various hydrothermal temperatures, showing that the calculated bandgap energy for all samples is shown in Table 1. This bandgap energy is optimal for visible light absorption, enabling BiOI to efficiently generate electron-hole pairs under solar illumination, which is essential for photocatalytic degradation processes [41]. The results indicate that BiOI is highly effective in degrading organic pollutants in wastewater, breaking harmful substances into harmless byproducts such as water and carbon dioxide. Furthermore, optimizing hydrothermal synthesis conditions plays a vital role in enhancing the structural and optical properties of BiOI, which improves its performance in solar-driven photocatalytic applications [42]. However, the bandgap energy alone cannot fully explain the differences in photocatalytic performance among the samples. Although the bandgap values of BiOI synthesized at 120°C, 150°C, and 210°C are quite similar, the superior activity observed in the 180°C sample is likely due to a combination of enhanced crystallinity and improved particle dispersion, which together contribute to better photocatalytic efficiency. The relationship between bandgap energy and photocatalytic performance will be further analyzed in the following section.

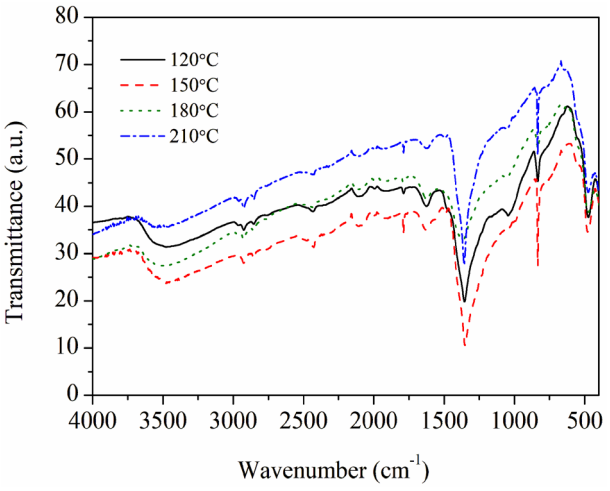

Figure 4. FT-IR spectra of BiOI synthesized by the hydrothermal process at different temperatures.

Additionally, the band edge position of BiOI is estimated by applying Mulliken electronegativity theory [37] as follows:

$$E_{VB} = X - E^e + 0.5E_g \quad (5)$$

$$E_{CB} = E_{VB} - E_g \quad (6)$$

where E_{VB} is the valence band edge potential. E_{CB} is the conduction band edge potential. X is absolute electronegativity and E_g is the bandgap energy of the semiconductor. E^e stands for the energy of free electrons on the hydrogen scale (about 4.5 eV). Other researchers have already obtained the X value for BiOI, which is 5.943 eV [37]. The calculated band edge positions of BiOI synthesized at different temperatures are summarized in Table 1. These values are crucial in determining the photocatalyst's ability to generate reactive oxygen species (ROS) during photocatalysis. Although the conduction band (CB) position of BiOI is more positive (+0.498 V vs. NHE) than the redox potential of $O_2/{}^{\bullet}O_2^-$ (–0.33 V), the possible generation of ${}^{\bullet}O_2^-$ may still be facilitated by high-energy photoexcited electrons or defect-mediated processes [39]. Similarly, the valence band (VB) position influences the oxidation potential of photogenerated h^+. If the VB is sufficiently positive, it can facilitate the formation of ${}^{\bullet}OH$, which are highly reactive and contribute significantly to pollutant degradation. The standard redox potentials for ${}^{\bullet}OH$ formation are +1.99 V vs. NHE from OH^- and +2.72 V vs. NHE from H_2O. Therefore, the VB of BiOI must be sufficiently positive to drive these oxidation reactions effectively [42].

PL spectra were measured to evaluate the charge carrier recombination behavior of BiOI samples shown in Figure 5(c). All samples exhibited a broad emission band centered around 590 nm and 620 nm, which is characteristic of BiOI and corresponds to the radiative recombination of photoinduced electron–hole pairs [43]. The sample synthesized at 120°C showed the lowest PL intensity, indicating suppressed recombination and enhanced charge separation

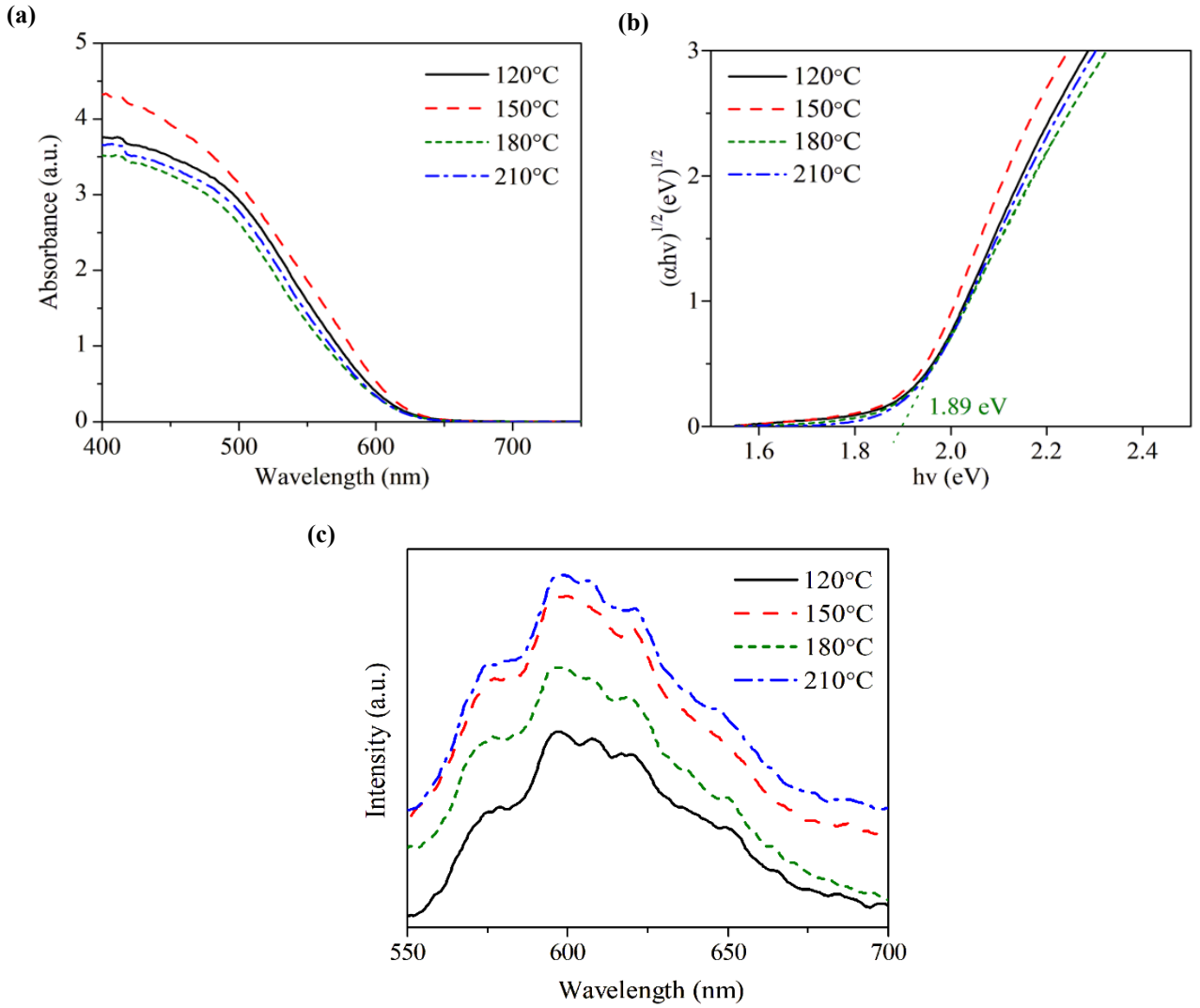

Figure 5. (a) UV–Vis diffuse reflectance spectra of BiOI samples synthesized by the hydrothermal process at different temperatures, (b) Tauc plots used to estimate the bandgap energy and (c) Photoluminescence spectra of BiOI samples synthesized at different hydrothermal temperatures.

3.5 Photocatalytic performance

The photocatalytic activity of BiOI samples synthesized at various hydrothermal temperatures was assessed through the degradation of indigo carmine under visible light. Figure 6(a) shows that the 180°C sample led to a notable reduction in absorbance at 610 nm, reflecting efficient dye removal. Although Brunauer–Emmett–Teller (BET) surface area data were not collected in this work, some differences in early-stage dye adsorption could be observed, particularly for the 150°C and 210°C samples (see Figure 6(c)). These differences may relate to surface structure as seen in the FE-SEM images. However, it should be emphasized that adsorption behavior alone does not determine the overall photocatalytic performance, which is also influenced by crystal quality and charge transport behavior.

Figure 6(b) compares the degradation efficiency among all four temperatures. The 180°C sample reached the highest removal rate (94% within 60 min). Meanwhile, Figure 6(c) presents the temporal changes in C/C_0. The k values were determined using the pseudo-first-order kinetic model (Equation (2)) based on $ln\left(\frac{C_0}{C}\right)$ versus time plots (not shown). The obtained values were 0.0512 min^{-1}, 0.0328 min^{-1}, 0.0564 min^{-1}, and 0.0479 min^{-1} for samples synthesized at 120°C, 150°C, 180°C, and 210°C, respectively. These values suggest that the 180°C sample had the most favorable reaction rate, with 120°C and 210°C following, while the 150°C sample showed the lowest value. This difference can be associated with a combination of factors, including crystallinity, particle arrangement, and interfacial interactions. Notably, although 150°C and 210°C showed reasonable dye uptake at the start, their overall efficiency remained lower, likely due to structural or electronic limitations.

As shown in Table 1, BiOI synthesized at 180°C exhibits the lowest bandgap energy (1.89 eV), which enhances visible light absorption and increases the number of photogenerated electron-hole pairs. This lower bandgap facilitates stronger photon absorption and promotes efficient charge excitation, thereby improving photocatalytic performance. Although the BiOI sample synthesized at 210°C showed the smallest particle size according to FE-SEM analysis, it also exhibited the highest photoluminescence (PL) intensity, indicating a higher rate of electron-hole recombination. Consequently, the photocatalytic efficiency of the 210°C sample was lower than that of the BiOI synthesized at 120°C. The enhanced activity of the 120°C sample can be attributed to its lower recombination rate, even though it exhibited more aggregated particles. In contrast, the BiOI synthesized at 180°C demonstrated a moderate PL intensity and a well-defined flower-like morphology, resulting in the highest photocatalytic activity among all samples. These findings suggest that achieving an optimal balance between charge separation and surface reactivity is crucial for maximizing photocatalytic efficiency [43].

To further contextualize the photocatalytic performance of the synthesized BiOI, Table 3 compares its degradation efficiency with previously reported nanomaterial-based photocatalysts. The results indicate that BiOI synthesized at 180°C in this study outperforms many previously reported nanomaterials for indigo carmine degradation, achieving higher efficiency in a shorter time. While some materials, such as Ni–$BaMo_3O_{10}$, exhibit slightly higher degradation efficiencies [44], they require a significantly longer reaction time (180 min). This highlights the effectiveness of synthesis temperature optimization in achieving rapid and efficient photocatalysis without additional dopants or composite formations. The findings from this study demonstrate that the optimal synthesis temperature for BiOI is 180°C, as it provides the best balance between crystallite size, charge separation efficiency, and surface characteristics. This result underscores the importance of synthesis conditions in tailoring the photocatalytic properties of BiOI, making it a promising candidate for practical environmental remediation applications.

3.6 Reusability of photocatalyst

The reusability of the photocatalyst is a critical factor for its practical application in the photocatalytic degradation of indigo carmine, offering a cost-effective and sustainable solution for wastewater treatment. This study evaluated BiOI synthesized at 180°C reusability over three consecutive cycles, as shown in Figure 7. The degradation efficiency of BiOI decreased from 94% in the fresh cycle to 85.7%, 77.5%, and 70.6% in the 1st, 2nd, and 3rd cycles, respectively. The observed decline in efficiency is primarily attributed to the accumulation of reaction residues on the catalyst surface and the partial structural degradation of BiOI, which may hinder light absorption and active site availability [22]. Despite the reduction in degradation efficiency over multiple cycles, BiOI retained significant photocatalytic performance under visible light irradiation, demonstrating its potential for practical wastewater treatment applications. The results indicate that BiOI synthesized via the hydrothermal method at an optimized temperature of 180°C can have multiple reuse cycles with acceptable efficiency [13].

Table 3. Comparison of the photocatalytic degradation efficiency of BiOI with previous studies.

Nanomaterial	Pollutant	Concentration	Photodegradation percentage/time	Reference
BiOI	Indigo carmine	5×10^{-5} M	94% within 60 min	This study
BiOI	Indigo carmine	20 $mg \cdot L^{-1}$	93% within 90 min	[13]
TiO_2: AC	Indigo carmine	5×10^{-5} M	71% within 90 min	[45]
$BaMo_3O_{10}$	Indigo carmine	20 $mg \cdot L^{-1}$	40% within 180 min	[44]
Ni–$BaMo_3O_{10}$	Indigo carmine	20 $mg \cdot L^{-1}$	98% within 180 min	[44]
Bi_2MoO_6	Indigo carmine	30 $mg \cdot L^{-1}$	94% within 120 min	[46]
BiOI	Rhodamine B	1×10^{-5} M	81% within 90 min	[47]

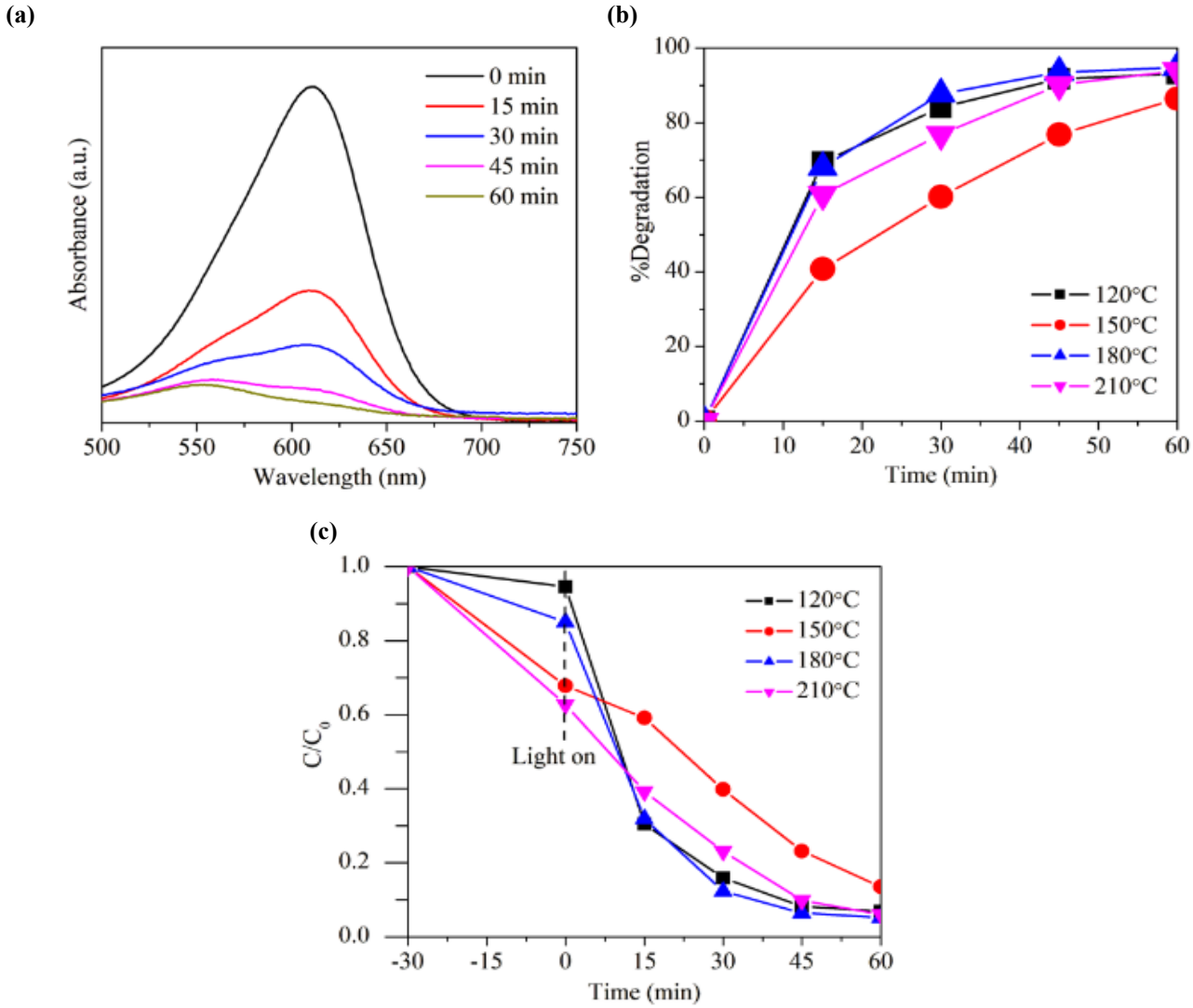

Figure 6. (a) Absorbance of indigo carmine solutions photocatalyzed by BiOI synthesized at 180°C, (b) Photocatalytic degradation efficiency of BiOI synthesized at different temperatures, and (c) Plots of C/C_0 for BiOI synthesized by hydrothermal process at different temperatures.

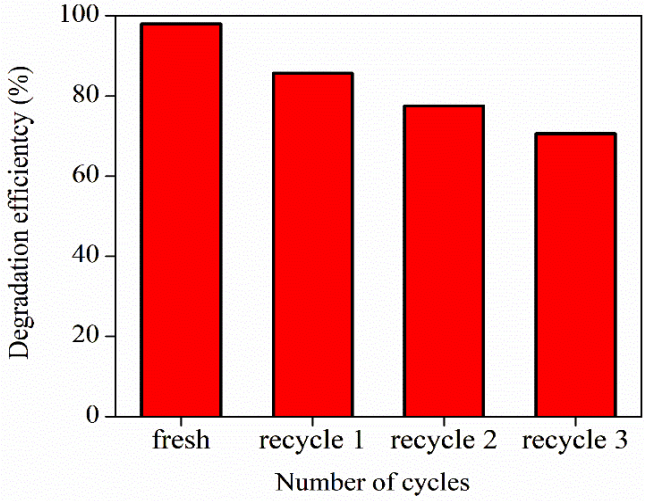

Figure 7. Cyclic runs for the degradation of indigo carmine on BiOI synthesized at 180°C

To enhance the long-term stability and performance of BiOI in cyclic use, further research could explore various regeneration strategies, such as surface cleaning techniques, structural reinforcement through doping, or composite formation, which could mitigate catalyst deactivation and extend its usability for additional cycles [48]. The decrease in photocatalytic efficiency over multiple cycles highlights the challenges associated with catalyst fouling and structural degradation. Catalyst poisoning due to the adsorption of organic intermediates and surface passivation can contribute to the loss of active sites and reduced charge separation efficiency [49]. However, the ability of BiOI to maintain over 70% efficiency after three cycles suggests that it is a viable option for practical environmental applications, with further optimization required to enhance durability.

3.7 Proposed mechanism

The photocatalytic degradation of indigo carmine by BiOI is primarily driven by $^{\bullet}O_2^-$, as indicated by the scavenger test results in

Figure 8. The significant reduction in photocatalytic activity when $^{\bullet}O_2^-$ scavengers are introduced confirms that these radicals play a crucial role in dye degradation. This observation initially appears inconsistent with the CB position of BiOI at +0.498 V (Table 1), which is more positive than the standard redox potential of $O_2/^{\bullet}O_2^-$ (–0.33 V). However, the generation of $^{\bullet}O_2^-$ confirmed by the scavenger experiment (Figure 8) may be attributed to defect-mediated charge transfer pathways that facilitate electron injection into molecular oxygen, as previously reported in BiOI systems with surface defects or oxygen vacancies [39]. These radicals facilitate the degradation of organic pollutants through oxidative pathways. Conversely, $^{\bullet}OH$ contributes minimally to the degradation process despite its high oxidation potential. This is unexpected given that the VB of BiOI at 2.398 eV is theoretically capable of oxidizing OH^- or water molecules into $^{\bullet}OH$, as their redox potentials (+1.99 eV and +2.27 eV, respectively) fall within the accessible range. However, the minimal impact of $^{\bullet}OH$ scavengers suggests that hydroxyl radicals are generated insufficiently or undergo rapid recombination before participating in dye oxidation. Even if some hydroxyl radicals form, their short lifetime and recombination with photogenerated electrons likely limit their effectiveness. One possible explanation is the relatively low density of surface hydroxyl groups, as observed in the FT-IR spectra (Figure 4), which reduces the availability of OH^- ions required for $^{\bullet}OH$ generation. Furthermore, the conduction band position of BiOI strongly favors O_2 reduction, making electron transfer to O_2 thermodynamically and kinetically more favorable than recombination with holes. As a result, BiOI-mediated photocatalysis under visible light predominantly follows an $^{\bullet}O_2^-$-driven mechanism rather than a hydroxyl radical-driven process. This insight is critical for designing BiOI-based photocatalysts optimized for different organic pollutant degradation pathways. Although h^+ possess strong oxidation potential, their contribution to the degradation process appears limited. One possible reason is that h^+ may undergo recombination with photogenerated electrons before participating in oxidation reactions. Additionally, due to the relatively low density of surface hydroxyl groups, direct oxidation of adsorbed dye molecules by h^+ may be inefficient compared to indirect oxidation through $^{\bullet}O_2^-$. The strong preference for the $^{\bullet}O_2^-$ pathway suggests that photogenerated h^+ either recombine rapidly or do not interact efficiently with surface species, reinforcing the $^{\bullet}O_2^-$-driven mechanism as the primary route for dye degradation in this system.

To better illustrate the proposed charge transfer pathways in BiOI synthesized at 180°C under visible light irradiation, Figure 9 presents a schematic representation of the photocatalytic mechanism. Based on the experimental findings, the photocatalytic degradation mechanism of indigo carmine using BiOI synthesized at different temperatures can be summarized as follows Equation (7-9);

$$\mathrm{BiOI} + h\nu \rightarrow e^- + h^+ \quad (7)$$

$$e^- + O_2 \rightarrow {}^{\bullet}O_2^- \quad (8)$$

$$^{\bullet}O_2^- + \text{indigo carmine} \rightarrow \text{Degraded products} \quad (9)$$

This mechanism underscores the dominant role of $^{\bullet}O_2^-$ in the degradation process and highlights the effectiveness of BiOI in utilizing visible light to generate active species for photocatalytic reactions.

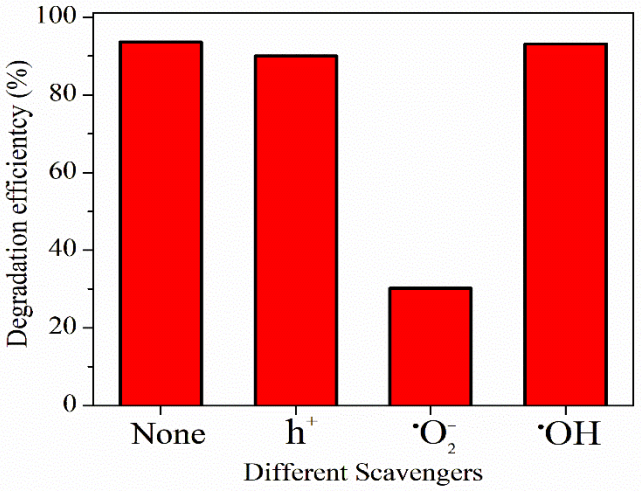

Figure 8. Effect of different scavengers on the removal efficiencies of indigo carmine by BiOI under visible light irradiation.

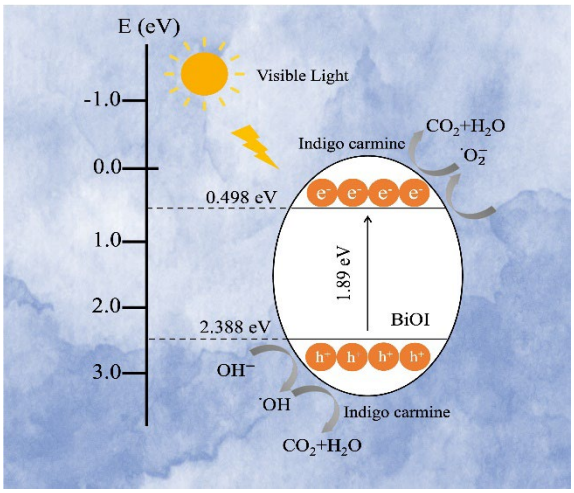

Figure 9. Proposed mechanism of charge transfer pathways in BiOI synthesized at 180°C under visible light irradiation.

4. Conclusions

This study systematically investigated the influence of hydrothermal synthesis temperature on the structural, optical, and photocatalytic properties of BiOI. XRD analysis confirmed that increasing the synthesis temperature enhanced crystallinity and grain growth, as evidenced by the higher intensity and sharper diffraction peaks, along with the largest crystallite size observed at 210°C. As determined by UV-vis and band structure calculations, the optical properties indicated that BiOI synthesized at 180°C possessed the lowest bandgap energy (1.89 eV), allowing enhanced visible-light absorption and effective charge carrier generation. The photocatalytic performance evaluation using indigo carmine degradation demonstrated that BiOI synthesized at 180°C achieved the highest degradation efficiency (94% within 60 min), attributed to its favorable microstructure and low recombination rate of electron and hole. Furthermore, mechanistic analysis using scavenger experiments identified $^{\bullet}O_2^-$ as the primary reactive species responsible for dye degradation. Despite the sufficient oxidation potential of the valence band for $^{\bullet}OH$ formation, their contribution to photocatalysis was minimal, likely due to the limited availability of

surface hydroxyl groups and a competitive electron transfer pathway favoring $^{\bullet}O_2^-$ generation. These results emphasize that synthesis temperature is a key parameter in optimizing BiOI photocatalysts, as it directly influences crystallinity, morphology, charge transfer properties, and reactive species generation. The findings provide valuable insights into designing efficient BiOI-based photocatalysts for wastewater treatment applications. This demonstrates that precise control over synthesis conditions can significantly enhance photocatalytic activity without requiring additional modifications such as elemental doping or heterostructure formation.

Acknowledgements

This work was supported by the Department of Physics, Faculty of Science, Silpakorn University.

References

[1] S. Jang, S. Song, J. H. Lim, H. S. Kim, B. T. Phan, K.-T. Ha, S. Park, and K. H. Park, "Application of various metal-organic frameworks (MOFs) as catalysts for air and water pollution environmental remediation," *Catalysts,* vol. 10, no. 2*,* 2020.

[2] O. Al-Madanat, Y. AlSalka, W. Ramadan, and D. W. Bahnemann, "TiO_2 photocatalysis for the transformation of aromatic water pollutants into fuels," *Catalysts,* vol. 11, no. 3*,* 2021.

[3] K. Singsumphan, C. Suwanchawalit, W. Somsorod, T. Sripathomkul, P. Sawanglap, K. Aiempanakit, and M. Aiempanakit, "Low-voltage electrophoretic deposition of silver nanoparticles on ZnO nanorods thin films for enhanced visible-light photocatalysis," *Optik,* vol. 322, p. 172179, 2025.

[4] Y. Pi, X. Li, Q. Xia, J. Wu, Y. Li, J. Xiao, and Z. Li, "Adsorptive and photocatalytic removal of persistent organic pollutants (POPs) in water by metal-organic frameworks (MOFs)," *Chemical Engineering Journal,* vol. 337, pp. 351-371, 2018.

[5] A. Talaiekhozani, S. Rezania, K.-H. Kim, R. Sanaye, and A. M. Amani, "Recent advances in photocatalytic removal of organic and inorganic pollutants in air," *Journal of Cleaner Production,* vol. 278, p. 123895, 2021.

[6] K. Wirandorn, N. Panyayao, and V. Siriwongrungson, "Characterization and photocatalytic activity of titanium dioxide deposited on stainless steel by pulsed-pressure MOCVD," *Journal of Metals, Materials and Minerals,* vol. 28, pp. 76-82, 2018.

[7] M. Aiempanakit, J. Sangkaworn, N. Worawannotai, K. Laohhasurayotin, W. Sangchay, S. Laksee, and C. Suwanchawalit, "Enhancement of visible light-responsive photocatalytic efficiency by using a laccaic acid-modified titanium dioxide photocatalyst," *Journal of the Brazilian Chemical Society,* vol. 33, 2022.

[8] F. Opoku, K. K. Govender, C. G. C. E. van Sittert, and P. P. Govender, "Recent progress in the development of semiconductor-based photocatalyst materials for applications in photocatalytic water splitting and degradation of pollutants," *Advanced Sustainable Systems,* vol. 1, no. 7, p. 1700006, 2017.

[9] X. Ren, J. Yao, L. Cai, J. Li, X. Cao, Y. Zhang, B. Wang, and Y. Wei, "Band gap engineering of BiOI via oxygen vacancies induced by graphene for improved photocatalysis," *New Journal of Chemistry,* vol. 43, no. 3, pp. 1523-1530, 2019.

[10] H. Liu, W. Cao, Y. Su, Y. Wang, and X. Wang, "Synthesis, characterization and photocatalytic performance of novel visible-light-induced Ag/BiOI," *Applied Catalysis B: Environmental,* vol. 111-112, pp. 271-279, 2012.

[11] S. Singh, R. Sharma, and M. Khanuja, "A review and recent developments on strategies to improve the photocatalytic elimination of organic dye pollutants by BiOX (X=Cl, Br, I, F) nanostructures," *Korean Journal of Chemical Engineering,* vol. 35, no. 10, pp. 1955-1968, 2018.

[12] M. Arumugam, and M. Y. Choi, "Recent progress on bismuth oxyiodide (BiOI) photocatalyst for environmental remediation," *Journal of Industrial and Engineering Chemistry,* vol. 81, pp. 237-268, 2020.

[13] M. R. Elamin, K. H. Ibnaouf, N. Y. Elamin, F. A. Adam, A. H. Alolayan, and B. Y. Abdulkhair, "Spontaneous adsorption and efficient photodegradation of indigo carmine under visible light by bismuth oxyiodide nanoparticles fabricated entirely at room temperature," *Inorganics,* 10, 2022.

[14] Y. Bu, J. Xu, Y. Li, Q. Liu, and X. Zhang, "Enhanced photocatalytic activity of BiOI under visible light irradiation by the modification of MoS_2," *RSC Advances,* vol. 7, no. 67, pp. 42398-42406, 2017.

[15] M. Chakraborty, K. K. Bera, S. Chatterjee, A. Ghosh, and S. K. Bhattacharya, "Synthesis of mesoporous BiOI flower and facile in-situ preparation of BiOI/BiOCl mixture for enhanced photocatalytic degradation of toxic dye, Rhodamine-B," *Journal of Photochemistry and Photobiology,* vol. 8, p. 100077, 2021.

[16] J.-w. Zhao, Z.-q. Wei, S.-p. Huang, L. Li, and J.-h. Ma, "Photocatalytic properties of bismuth oxyiodide nanomaterials with different morphologies," *Desalination and Water Treatment,* vol. 281, pp. 287-295, 2023.

[17] W. W. Lee, C.-S. Lu, C.-W. Chuang, Y.-J. Chen, J.-Y. Fu, C.-W. Siao, and C.-C. Chen, "Synthesis of bismuth oxyiodides and their composites: characterization, photocatalytic activity, and degradation mechanisms," *RSC Advances,* vol. 5, no. 30, pp. 23450-23463, 2015.

[18] H. Liu, C. Yang, J. Huang, J. Chen, J. Zhong, and J. Li, "Ionic liquid-assisted hydrothermal preparation of BiOI/BiOCl heterojunctions with enhanced separation efficiency of photogenerated charge pairs and photocatalytic performance," *Inorganic Chemistry Communications,* vol. 113, p. 107806, 2020.

[19] D. Ke, T. Peng, L. Ma, P. Cai, and K. Dai, "Effects of hydrothermal temperature on the microstructures of $BiVO_4$ and Its photocatalytic O_2 evolution activity under visible light," *Inorganic Chemistry,* vol. 48, no. 11, pp. 4685-4691, 2009.

[20] S. Wang, Y. Guan, L. Wang, W. Zhao, H. He, J. Xiao, S. Yang, and C. Sun, "Fabrication of a novel bifunctional material of BiOI/Ag_3VO_4 with high adsorption–photocatalysis for efficient treatment of dye wastewater," *Applied Catalysis B: Environmental,* vol. 168-169, pp. 448-457, 2015.

[21] B. Q. L. Low, W. Jiang, J. Yang, M. Zhang, X. Wu, H. Zhu, H. Zhu, J. Z. X. Heng, K. Y. Tang, W.-Y. Wu, X. Cao, X. Q. Koh, C. H. T. Chai, C. Y. Chan, Q. Zhu, M. Bosman, Y.-W. Zhang, M. Zhao, Z. Li, X. J. Loh, Y. Xiong, and E. Ye, "2D/2D heterojunction of BiOBr/BiOI nanosheets for in situ H_2O_2 production and activation toward efficient photocatalytic waste-

water treatment," *Small Methods,* vol. 8, no. 3, p. 2301368, 2024.

[22] M. Yusoff, S. Imam, I. Shah, and R. Adnan, "Photocatalytic activity of bismuth oxyiodide nanospheres and nanoplates in the degradation of ciprofloxacin under visible light," *Materials Research Express,* vol. 6, 2019.

[23] J. Florez, M. A. Santana Aranda, J. G. Quiñones-Galván, A. Escobedo Morales, A. Chavez Chavez, and A. Pérez-Centeno, "Alternative Bi precursor effects on the structural, optical, morphological and photocatalytic properties of BiOI nanostructures," *Materials Research Express,* vol. 7, p. 015912, 2020.

[24] T. Gupta, Samriti, J. Cho, and J. Prakash, "Hydrothermal synthesis of TiO_2 nanorods: formation chemistry, growth mechanism, and tailoring of surface properties for photocatalytic activities," *Materials Today Chemistry,* vol. 20, p. 100428, 2021.

[25] X.-D. Dong, Y.-M. Zhang, and Z.-Y. Zhao, "Role of the polar electric field in bismuth oxyhalides for photocatalytic water splitting," *Inorganic Chemistry,* vol. 60, no. 12, pp. 8461-8474, 2021.

[26] R. He, S. Cao, J. Yu, and Y. Yang, "Microwave-assisted solvothermal synthesis of $Bi_4O_5I_2$ hierarchical architectures with high photocatalytic performance," *Catalysis Today,* vol. 264, 2015.

[27] H. Li, Q. Jia, Y. Cui, and S. Fan, "Photocatalytic properties of BiOI synthesized by a simple hydrothermal process," *Materials Letters,* vol. 107, pp. 262-264, 2013.

[28] Z. Zulkifli, K. Razak, and W. Rahman, *The effect of reaction temperature on the particle size of bismuth oxide nanoparticles synthesized via hydrothermal method*, 2018.

[29] F. Huang, H. Zhang, and J. F. Banfield, "Two-stage crystal-growth kinetics observed during hydrothermal coarsening of nano-crystalline ZnS," *Nano Letters,* vol. 3, no. 3, pp. 373-378, 2003.

[30] M. Aiempanakit, P. Sudjai, K. Singsumphan, S. Laksee, and C. Suwanchawalit, "Brazilein modified zinc oxide nanorods with enhanced visible light-responsive photocatalytic efficiency," *Journal of Metals, Materials and Minerals,* vol. 32, pp. 70-76, 2022.

[31] Y.-S. Cho, H. J. Lee, and S. Sung, "Photocatalytic degradation of methylene blue using three-dimensional porous graphene-titania microparticles under UV light," *Korean Journal of Chemical Engineering,* vol. 37, no. 6, pp. 1071-1085, 2020.

[32] A. C. Mera, Y. Moreno, D. Contreras, N. Escalona, M. F. Meléndrez, R. V. Mangalaraja, and H. D. Mansilla, "Improvement of the BiOI photocatalytic activity optimizing the solvothermal synthesis," *Solid State Sciences,* vol. 63, pp. 84-92, 2017.

[33] H. H. Yang, K.-Y. Hsiao, F.-Y. Liu, C.-C. Chen, and I. C. Chen, "Vibrational structures of iodine-vacancy bismuth oxyiodides using temperature-dependent low-wavenumber raman spectroscopy," *The Journal of Physical Chemistry C,* vol. 128, no. 1, pp. 563-570, 2024.

[34] A. C. Mera, C. Rodríguez, M. Meléndrez, and H. Valdes, "Synthesis and characterization of BiOI microspheres under standardized conditions," *Journal of Materials Science,* vol. 52, 2017.

[35] S. Bhattacharjee, C. R. Macintyre, X. Wen, P. Bahl, U. Kumar, A. A. Chughtai, and R. Joshi, "Nanoparticles incorporated graphene-based durable cotton fabrics," *Carbon,* vol. 166, pp. 148-163, 2020.

[36] J. Wang, M. Zhang, J. Meng, Q. Li, and J. Yang, "Single- and few-layer BiOI as promising photocatalysts for solar water splitting," *RSC Advances,* vol. 7, no., pp. 24446-24452, 2017.

[37] A. C. Mera, A. Martínez-de la Cruz, E. Pérez-Tijerina, M. F. Meléndrez, and H. Valdés, "Nanostructured BiOI for air pollution control: Microwave-assisted synthesis, characterization and photocatalytic activity toward NO transformation under visible light irradiation," *Materials Science in Semiconductor Processing,* vol. 88, pp. 20-27, 2018.

[38] M. Riebe, D. Foustoukos, C. Alexander, A. Steele, G. Cody, B. Mysen, and L. Nittler, *The effects of atmospheric entry heating on organic matter in interplanetary dust particles*, 2020.

[39] J. Bai, J. Sun, X. Zhu, J. Liu, H. Zhang, X.-B. Yin, and L. Liu, "Enhancement of solar-driven photocatalytic activity of bioi nanosheets through predominant exposed high energy facets and vacancy engineering," *Small,* vol. 16, no. 5, p. 1904783, 2020.

[40] L. Dou, D. Ma, J. Chen, J. Li, and J. Zhong, "F127-assisted hydrothermal preparation of BiOI with enhanced sunlight-driven photocatalytic activity originated from the effective separation of photo-induced carriers," *Solid State Sciences,* vol. 90, pp. 1-8, 2019.

[41] L. Ye, K. Deng, F. Xu, L. Tian, T. Peng, and L. Zan, "Increasing visible-light absorption for photocatalysis with black BiOCl," *Physical Chemistry Chemical Physics,* vol. 14, no. 1, pp. 82-85, 2012.

[42] J. Li, J. Zhong, Y. Si, S. Huang, L. Dou, M. Li, Y. Liu, and J. Ding, "Improved solar-driven photocatalytic performance of BiOI decorated TiO_2 benefiting from the separation properties of photo-induced charge carriers," *Solid State Sciences,* vol. 52, pp. 106-111, 2016.

[43] Y. Bu, J. Xu, Y. Li, Q. Liu, and X. Zhang, "Enhanced photocatalytic activity of BiOI under visible light irradiation by the modification of MoS_2," *RSC Advances.,* vol. 7, pp. 42398-42406, 2017.

[44] S. K. Ray, D. Dhakal, and S. W. Lee, "Visible light driven Ni–$BaMo_3O_{10}$ photocatalyst for indigo carmine degradation: mechanism and pathways," *Materials Science in Semiconductor Processing,* vol. 105, p. 104697, 2020.

[45] A. K. Subramani, K. Byrappa, S. Ananda, K. M. Lokanatha Rai, C. Ranganathaiah, and M. Yoshimura, "Photocatalytic degradation of indigo carmine dye using TiO_2 impregnated activated carbon," *Bulletin of Materials Science,* vol. 30, no. 1, pp. 37-41, 2007.

[46] C. Sánchez Trinidad, A. Martínez-de la Cruz, and E. López Cuéllar, "Photocatalytic degradation of indigo carmine by hydrothermally synthesized Bi_2MoO_6 in presence of EDTA," *Environmental Science and Pollution Research,* vol. 22, no. 2, pp. 792-799, 2015.

[47] P. Intaphong, A. Phuruangrat, S. Thongtem, and T. Thongtem, "Sonochemical synthesis and characterization of BiOI nano-

plates for using as visible-light-driven photocatalyst," *Materials Letters,* vol. 213, pp. 88-91, 2018.

[48] Q. Wang, H. Wu, Q. Gao, D. Lin, Y. Fan, R. Duan, Y. Cong, and Y. Zhang, "Fabrication of visible-light-active Bi/BiOI-Bi_2O_3 composite with enhanced photocatalytic activity," *Journal of Colloid and Interface Science,* vol. 548, pp. 255-264, 2019.

[49] J. Shi, X. Zhao, and C. Li, "Surface passivation engineering for photoelectrochemical water splitting," *Catalysts,* 13, 2023.